# Multifragmentation
# in Relativistic Heavy Ion Reactions*

W. Trautmann
Gesellschaft für Schwerionenforschung mbH
D-64291 Darmstadt, Germany

**Abstract**

Multifragmentation is the dominant decay mode of heavy nuclear systems with excitation energies in the vicinity of their binding energies. It explores the partition space associated with the number of nucleonic constituents and it is characterized by a multiple production of nuclear fragments with intermediate mass.

Reactions at relativistic bombarding energies, exceeding several hundreds of MeV per nucleon, have been found very efficient in creating such highly excited systems. Peripheral collisions of heavy symmetric systems or more central collisions of mass asymmetric systems produce spectator nuclei with properties indicating a high degree of equilibration. The observed decay patterns are well described by statistical multifragmentation models.

The present experimental and theoretical studies are particularly motivated by the fact that multifragmentation is being considered a possible manifestation of the liquid-gas phase transition in finite nuclear systems. From the simultaneous measurement of the temperature and of the energy content of excited spectator systems a caloric curve of nuclei has been obtained. The characteristic S-shaped behavior resembles that of ordinary liquids.

Signatures of critical phenomena in finite nuclear systems are searched for in multifragmentation data. These studies, supported by the success of percolation in reproducing the experimental mass or charge correlations, concentrate on the fluctuations observed in these observables. Attempts have been made to deduce critical-point exponents associated with multifragmentation.

*Lecture Notes of NATO Advanced Study Institute, Dronten, The Netherlands, 1996, to appear in *Correlations and Clustering Phenomena in Subatomic Physics*, edited by M.N. Harakeh, O. Scholten, and J.K. Koch, Plenum Publishing Corporation.

# 1 Introduction

The hope to establish a link to the liquid-gas phase transition in nuclear matter has been a major motivation for the search for and the study of multi-fragment decays of heavy nuclei in recent years [1, 2]. Multifragmentation was predicted to be the dominant decay mode at excitation energies near the binding energy of nuclei of about 8 MeV per nucleon and at densities below the saturation density of nuclear matter [3, 4]. These conditions of high excitation and low density coincide with the liquid-gas coexistence region as predicted for nuclear matter from the Van-der-Waals type range dependence of the nuclear forces [5, 6]. It was also suggested early on that this region may be explored during the later stages of energetic nuclear reactions [7].

The experimental study of the nuclear liquid-gas phase transition in finite nuclei faces several serious difficulties related to the fact that excited nuclei are composed of a small number of constituents, that they are charged, and that there is no external pressure to counteract the internal pressure of the system at a given equilibrium condition [8]. Finite pressures may be maintained only dynamically and for very short periods of time during the disintegration process. There is also no heat bath available which would allow to predetermine the temperature of the system in order to measure its response to it.

In spite of these difficulties, stimulating new results have been presented very recently. They suggest that signals of the nuclear liquid-gas phase transition may be revealed by studying reactions of finite nuclei. From the simultaneous measurement of the temperature and the excitation energy for excited projectile spectators in $^{197}$Au + $^{197}$Au collisions at 600 MeV per nucleon a caloric curve of nuclei has been obtained [9]. It exhibits a typical S-shaped behavior, reminiscent of first-order phase transitions in macroscopic systems. For the $^{197}$Au on C reaction at 1.0 GeV per nucleon, the EOS collaboration has reported values of critical-point exponents which were derived from the correlations and fluctuations of the fragment sizes [10]. In both cases, the data providing the basis for the analysis were obtained from the fragmentation of heavy projectiles at relativistic energies in the range of up to about 1 GeV per nucleon. The decay properties of spectator nuclei produced in these reactions indicate that a high degree of equilibrium has been reached. This is a prerequisite for the study of the thermodynamic behavior of highly excited nuclear matter and makes these reactions rather attractive for this purpose.

In the following notes, some main features of multifragment-decays following heavy-ion reactions in the relativistic regime of bombarding energies will be summarized. The experimental material will be mostly taken from the work of the ALADIN collaboration, performed at the heavy-ion synchrotron SIS of the GSI in Darmstadt [11, 12]. The techniques used to determine the observables related to the liquid-gas phase transition will be

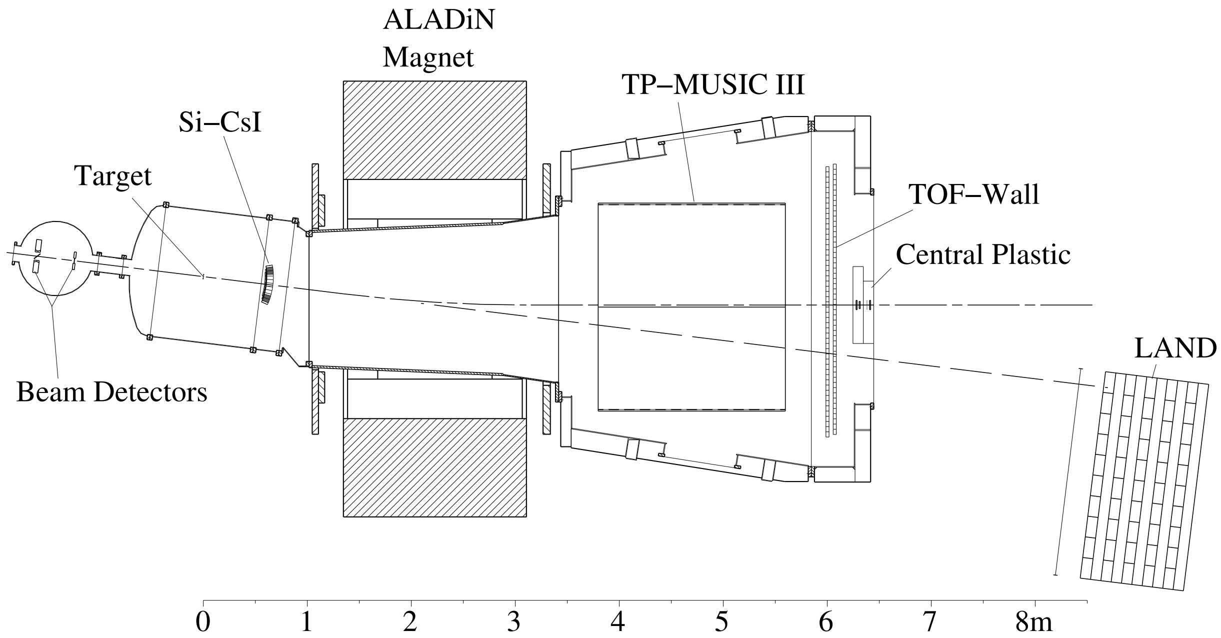


Figure 1: Cross sectional view of the ALADIN facility in the configuration of the 1993 experiment. The beam enters from the left and is monitored by two beam detectors before reaching the target. Projectile fragments entering into the acceptance of the magnet are tracked and identified in the TP-MUSIC III detector and in the time-of-flight (TOF) wall. The Central Plastic detector covers the hole in the TOF wall at the exit for the beam. Fragments and particles emitted in forward directions outside the magnet acceptance and up to $\theta_{lab} = 16°$ are detected in the Si-CsI array. Neutrons emitted in directions close to $\theta_{lab} = 0°$ are detected with the large-area neutron detector (LAND). The dashed line indicates the direction of the incident beam. The dash-dotted line represents the trajectory of beam particles after they were deflected by an angle of 7.3° (from Ref. [11]).

briefly described. It is not intended, however, to give a complete account of the present discussion initiated by these results. Besides the references cited, the reader is referred to the proceedings of recent conferences or workshops [13-16] during which the topic has been discussed within a wider perspective. Further references on the subject of multifragmentation in general may be found in [17].

## 2 Experimental study of projectile decay

The first observations of multi-fragment decays of heavy projectiles have been made by exposing nuclear emulsions to the heavy ion beams [18, 19]. This technique is still being used and, just recently, has produced first results on the fragmentation of gold nuclei at the energy of 10.6 GeV per nucleon, available from the AGS in Brookhaven [20, 21]. Another

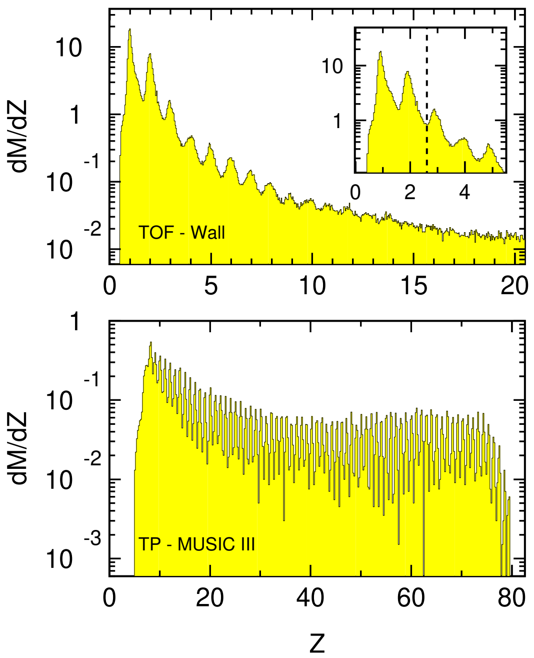


Figure 2: $Z$-identification spectra measured with the TOF wall (top) and the TP-MUSIC (bottom) for the reaction $^{197}$Au on $^{197}$Au at $E/A = 600$ MeV. The $Z$ information from the TP-MUSIC was used to calibrate the response of the TOF wall in the region $Z > 15$. Note that the element yield at $Z > 65$ is affected by the experimental trigger.
Insert: Low-$Z$ part of the TOF-wall spectrum. The dashed line indicates the equivalent sharp cut which was used for selecting fragments with $Z \geq 3$ (from Ref. [11]).

technique, employed in several studies, is based on plastic nuclear track detectors which have high charge resolution for atomic numbers $Z \geq 6$ [22].

More detailed investigations are possible with electronic detection devices such as the ALADIN spectrometer at SIS [11, 23]. This detector system is built around A Large Acceptance DIpole magNet (ALADIN) with the target in front of the magnetic-field gap and the main detector systems behind it. The configuration used in the 1993 experiment, a systematic study covering a wide range of beams and targets, is shown in Fig. 1. In this experiment, complete acceptance within the kinematic region of projectile decay with good resolution was achieved. The solid angle adjacent to the acceptance of the ALADIN magnet was covered with 84 Si-CsI(Tl) telescopes in closely packed geometry. Behind the magnet, the MUltiple Sampling Ionization Chamber (MUSIC) served as the tracking detector. The high charge resolution of this detector permitted the identification of individual elements above a threshold atomic number $Z \geq 8$ (Fig. 2, bottom panel). Lighter fragments were tracked and identified by collecting and amplifying their ionization charges with propor-

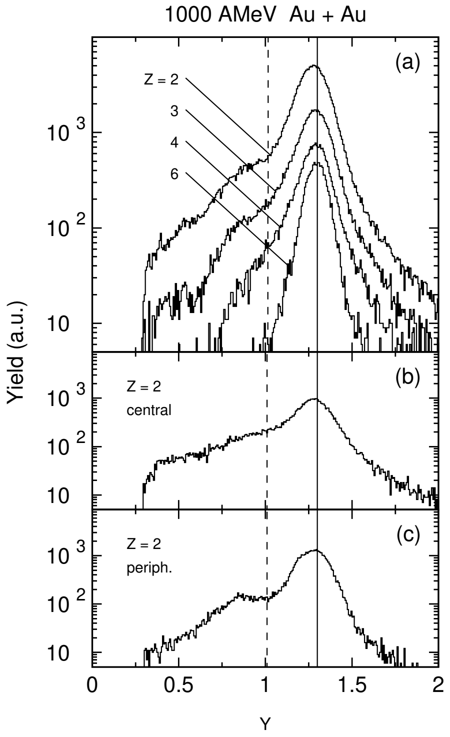


Figure 3: (a): Rapidity spectra measured in the reaction $^{197}$Au on $^{197}$Au at $E/A$ = 1000 MeV for fragments with $Z$ = 2, 3, 4, and 6. The solid and dashed lines indicate the measured most probable rapidity $y$ = 1.32 of the light fragments and the condition $y \geq 0.75 \cdot y_P$ adopted for fragments from the projectile spectator, respectively.
(b): Rapidity spectra of helium fragments, measured in central collisions ($Z_{bound} \leq 30$) for the same reaction.
(c): Same as (b) for peripheral collisions ($Z_{bound} \geq 50$) (from Ref. [11]).

tional counters mounted in three positions at the anode plane of the drift volume.

The two-layered time-of-flight (TOF) wall extended over 2.4 m in the horizontal and 1.0 m in the vertical directions. Fragments with $Z \leq 15$ were elementally resolved with the TOF wall detectors (Fig. 2, top panel). The resolution of the time-of-flight measurement with respect to the beam detectors positioned upstream was between 200 ps and 400 ps (FWHM), depending on the fragment $Z$. It permitted the determination of the individual masses of the lighter products with $Z$ up to about 12 from the momenta given by the tracking analysis. In addition to the charged projectile fragments, neutrons emitted in directions close to $\Theta_{lab} = 0°$ were measured with the Large-Area Neutron Detector (LAND) which was operated in a calorimetric mode.

The fragments from the decay of excited projectile spectators are well localized in rapidity. This is illustrated in Fig. 3 where rapidity spectra of light fragments from the reaction $^{197}$Au on $^{197}$Au at $E/A = 1000$ MeV are shown. The distributions are concentrated around a rapidity value very close to that of the projectile, $y_P$, and become increasingly narrower with increasing mass of the fragment. For the lighter fragments, the distributions extend into the mid-rapidity region. The widths and shapes of the distributions also depend on the impact parameter, as demonstrated for helium fragments in the two lower panels of Fig. 3. The bump in the peripheral He spectrum, located at a rapidity $y$ between 0.8 and 0.9, and similar bumps observed for light fragments up to $Z \approx 4$ (Fig. 3, top) originate from mid-rapidity emission.

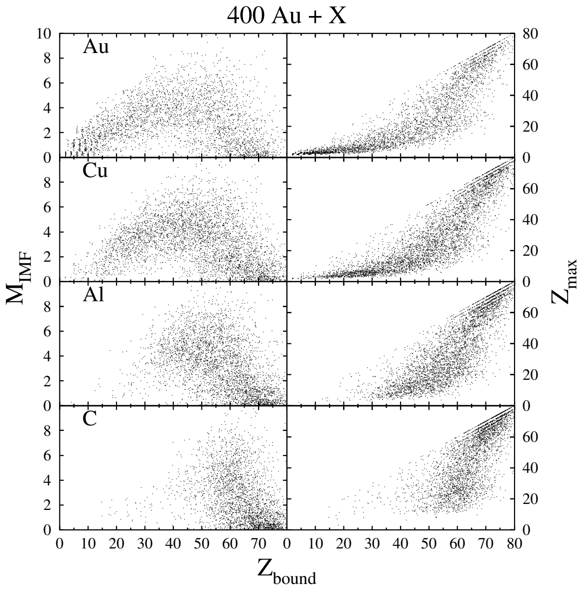


Figure 4: Multiplicity of intermediate-mass fragments (left-hand side) and atomic number of the largest fragment (right-hand side) as a function of $Z_{bound}$ for the reaction $^{197}$Au on $^{197}$Au at $E/A$ = 400 MeV. Random numbers, taken from the interval [-0.5,0.5], were added to the integer values $M_{IMF}$ in order to preserve the intensity information in the scatter plot (from Ref. [24]).

Based on these observations and on model studies, limits for the kinematic region of the projectile source were chosen for the off-line analysis. The condition $y \geq 0.75 \cdot y_P$ was adopted for the fragment rapidities (cf. Fig. 3), and upper limits in the laboratory angle were set which took the observed invariance of the transverse fragment momenta with bombarding energy into account. These definitions permitted a comparison of data measured at different bombarding energies on a quantitative level [11].

## 3 Universality of spectator decay

The decay of excited spectators exhibits universal features which become apparent in the observed $Z_{bound}$ scaling of the measured charge correlations. The quantity $Z_{bound}$ is defined as the sum of the atomic numbers $Z_i$ of all projectile fragments with $Z_i \geq 2$. It represents the charge of the original spectator system reduced by the number of hydrogen isotopes emitted during its decay.

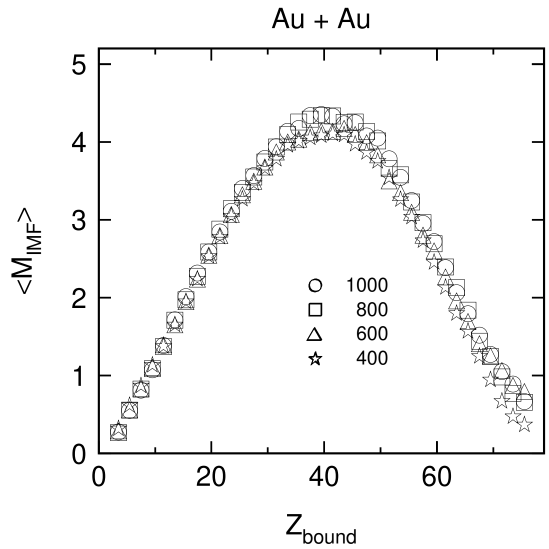


Figure 5: Mean multiplicity of intermediate-mass fragments $\langle M_{IMF} \rangle$ as a function of $Z_{bound}$ for the reaction $^{197}$Au on $^{197}$Au at $E/A$ = 400, 600, 800, and 1000 MeV (from Ref. [11]).

Scatter plots of two charge observables, the multiplicity $M_{IMF}$ of intermediate-mass fragments (IMFs, $3 \leq Z \leq 30$) and the maximum fragment charge $Z_{max}$ within the event, are shown in Fig. 4 as a function of $Z_{bound}$ for $^{197}$Au projectiles at 400 MeV per nucleon incident energy. The four rows of panels correspond to the results obtained with the four targets C, Al, Cu, and Au. It follows from the geometric properties of heavy-ion reactions at these energies that the mass (or charge) of the spectator, and therefore also $Z_{bound}$, is closely related to the impact parameter. At large $Z_{bound}$, the number of fragments is small and mainly one heavy residue nucleus with $Z_{max} \approx Z_{bound}$ is produced. With decreasing $Z_{bound}$ the number of fragments increases and, correspondingly, $Z_{max}$ is considerably smaller than $Z_{bound}$. Multi-fragment production dominates for impact parameters corresponding to $Z_{bound} \approx 40$. In central collisions with the heavier targets, the region of small $Z_{bound}$ is strongly populated. Here both $M_{IMF}$ and $Z_{max}$ decrease, reflecting the smaller size of the spectators produced in these collisions. This behavior was termed the rise and fall

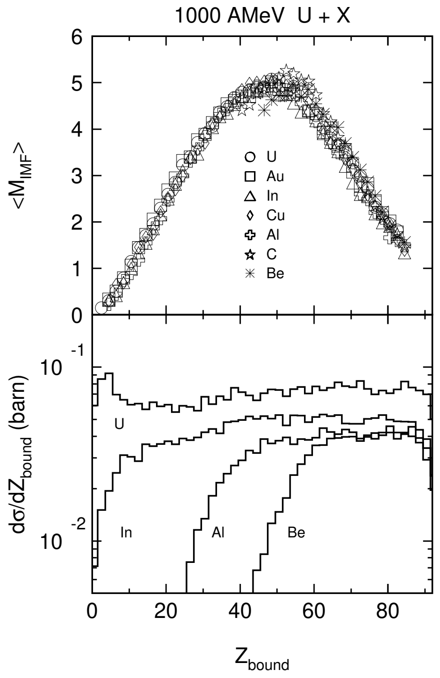


Figure 6: Top: Mean multiplicity of intermediate-mass fragments $\langle M_{IMF}\rangle$ as a function of $Z_{bound}$ for the reactions of $^{238}$U projectiles at $E/A$ = 1000 MeV with the seven targets Be, C, Al, Cu, In, Au, and U.
Bottom: Measured cross sections $d\sigma/dZ_{bound}$ for the reactions of $^{238}$U projectiles at $E/A$ = 1000 MeV with the four targets Be, Al, In, and U. Note that the experimental trigger, for the case of uranium beams, affected the cross sections for $Z_{bound} \geq 70$ (from Ref. [11]).

of multi-fragment emission [25]. On the side of the rise, at large $Z_{bound}$, the fragment production is governed by the amount of deposited energy, whereas in the fall region the limit of unconditional partitioning is approached [26].

The almost identical behavior of the observed charge correlations for different reactions, already suggested by the scatter plots, is best appreciated when looking at the mean values of these observables: In Fig. 5 the mean number of intermediate-mass fragments is shown as a function of $Z_{bound}$ for the reaction of $^{197}$Au on $^{197}$Au at four bombarding energies. The rise and fall of fragment production is seen to be independent of the projectile energy within the experimental accuracy. This invariance also holds for other charge correlations that have been found useful to characterize the population of the partition space in the fragmentation process [11, 27].

The target invariance of the $M_{IMF}$ versus $Z_{bound}$ correlation was first observed for collisions of $^{197}$Au projectiles with C, Al, Cu, and Pb targets at 600 MeV per nucleon [23,25-27]. In Fig. 6 (top) the universal nature of this correlation is demonstrated for $^{238}$U projectiles

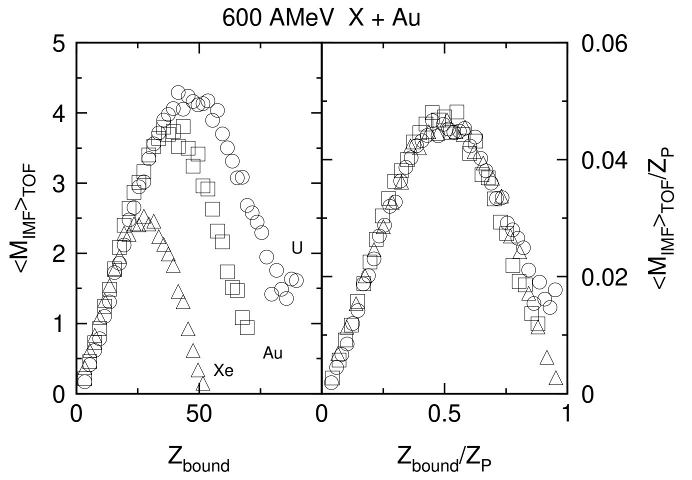


Figure 7: Left panel: Mean multiplicity of intermediate-mass fragments $\langle M_{IMF} \rangle_{TOF}$, observed with the TOF wall, as a function of $Z_{bound}$ for the reactions $^{238}$U on $^{197}$Au (circles), $^{197}$Au on $^{197}$Au (squares), and $^{129}$Xe on $^{197}$Au (triangles) at $E/A$ = 600 MeV. Note that also in $Z_{bound}$ only fragments detected with the TOF wall are included.
Right panel: The same data, as shown in the left panel, after normalizing both quantities with respect to the atomic number $Z_P$ of the projectile (from Ref. [11]).

at 1000 MeV per nucleon and for a set of seven targets, ranging from Be to U. The data for the lighter targets extend only over parts of the $Z_{bound}$ range. This is more clearly seen in the bottom part of the figure where the differential cross sections $d\sigma/dZ_{bound}$ for four out of the seven targets are shown. From the cross sections, by assuming a monotonic relation between $Z_{bound}$ and the impact parameter, an empirical impact parameter scale was obtained. Central collisions correspond to the smallest values of $Z_{bound}$ reached with a given target, and given regions of $Z_{bound}$, in collisions with different targets, correspond to different impact parameters. The cross sections were found to depend somewhat on the bombarding energy. The range of $Z_{bound}$ covered with, e.g., the Be or C targets increases with increasing bombarding energy.

The $\langle M_{IMF} \rangle$ versus $Z_{bound}$ correlation depends on the mass of the projectile. The results obtained with the three projectiles $^{129}$Xe, $^{197}$Au, and $^{238}$U at 600 MeV per nucleon show that, on the absolute scale, more fragments are produced in the decay of heavier projectiles (Fig. 7, left-hand side). However, a normalization with respect to the atomic number $Z_P$ of the projectile reduces the three curves to a single universal relation (Fig. 7, right-hand side).

The observed $Z_{bound}$ scaling thus comprises the dependences on the projectile and target mass and on the bombarding energy. The data obtained at the AGS with beams of 10.6

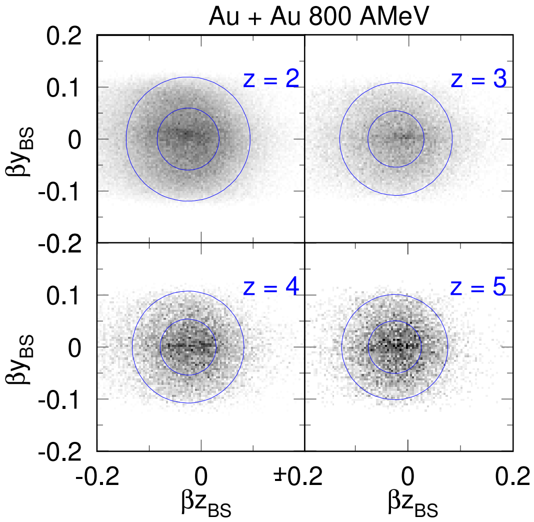


Figure 8: Projections of the fragment velocity $\beta_{BS}$ in the moving frame (BS = beam system) into the y-z-plane for products with atomic number $Z$ = 2 to 5 from the reaction $^{197}$Au on $^{197}$Au at $E/A$ = 800 MeV (y and z denote the directions parallel to the magnetic field and along the beam direction, respectively). The component $\beta y_{BS}$ is limited by the vertical acceptance of the magnet, the circles are meant to guide the eye (from Ref. [30]).

GeV per nucleon, in fact, indicate that it should be valid up to very high bombarding energies [20, 21]. The reasons underlying this property of spectator decay may be sought in the mechanism of spectator excitation. Calculations with the intranuclear cascade model [28] suggest that the relation between the excitation energy and the residual mass of the spectator should be universal [11, 29]. In this case, if the subsequent decay proceeds statistically, the final fragmentation patterns will only depend on $Z_{bound}$ and not on the particular entrance channel of the reaction.

# 4 The equilibrated spectator source

The observed universality of the spectator decay suggests that a high degree of equilibrium is reached in the initial stages of the reaction. This is confirmed by the analysis of the kinetic variables in the moving frame of the spectator.

The times and positions measured with the TOF wall were used to calculate the components of the fragment velocities in the reference frame of the original projectile. Results obtained for light fragments from the reaction $^{197}$Au on $^{197}$Au at $E/A$ = 800 MeV are

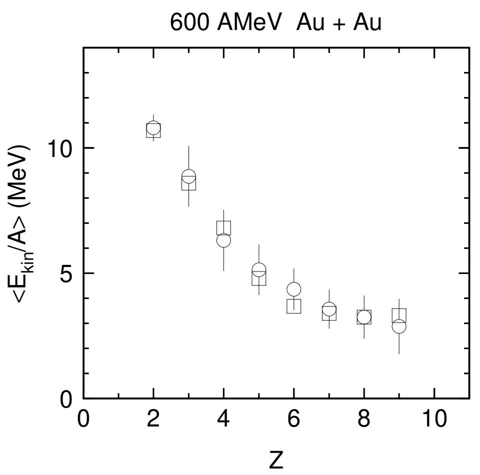


Figure 9: Mean kinetic energies per nucleon in the moving frame, deduced from the transverse (circles) and longitudinal (squares) momentum widths, for fragments from the reaction $^{197}$Au on $^{197}$Au at $E/A = 600$ MeV and for $20 \leq Z_{bound} \leq 60$ (from Ref. [11]).

shown in Fig. 8. In the y direction, the acceptance of the magnet limits the observable range of velocities. Apart from this, the distributions are seen to be isotropic to a very good approximation. Gaussian widths fitted to the measured distributions of the velocity components in the moving frame confirm this isotropy quantitatively.

The intrinsic velocities have also been used to determine the fragment kinetic energies in the frame of the decaying spectator. Results for the reaction $^{197}$Au on $^{197}$Au at 600 MeV per nucleon, integrated over $20 \leq Z_{bound} \leq 60$, are shown in Fig. 9. It was assumed that either the longitudinal (squares) or the vertical transverse (circles) degrees of freedom represent one third of the total kinetic energies in the moving frame. The agreement between the two sets of results reflects the isotropy of the kinetic degrees of freedom. The intrinsic kinetic energies do not depend on the bombarding energy and thus are representative for the whole energy range over which the universal spectator decay prevails.

The mean kinetic energies per unit fragment mass $\langle E_{kin}/A \rangle$ decrease rapidly with atomic number $Z$. In the limit of purely thermal contributions to the kinetic energies, $\langle E_{kin}/A \rangle$ is expected to have a $1/A$ dependence which is approximately observed. However, on the order of one half of the kinetic energies in the rest frame of the decaying system may originate from Coulomb repulsion and sequential decays of excited fragments [31]. With this assumption the magnitude of the kinetic temperature $T = 2/3 \cdot 1/2 \cdot \langle E_{kin} \rangle$ assumes a value of approximately 15 MeV. This exceeds considerably the emission temperatures $T \approx 5$ MeV derived from the relative isotopic abundances (see below) or from relative yields of particle unbound states [32] which represents a well known but up to now not fully resolved problem [33-36].

# 5 Temperatures at breakup

Several techniques have been developed for the measurement of temperatures of excited nuclear systems [37]. In the work leading to the caloric curve of nuclei the method suggested by Albergo *et al.* [38] has been used. It is based on the assumption of chemical equilibrium and requires the measurement of double ratios of isotopic yields.

In the limit of thermal and chemical equilibrium, the double ratio $R$ built from the yields $Y_i$ of two pairs of nuclides with the same differences in neutron and proton numbers is given by

$$R = \frac{Y_1/Y_2}{Y_3/Y_4} = a \cdot \exp(((B_1 - B_2) - (B_3 - B_4))/T) \tag{1}$$

where $B_i$ denotes the binding energy of particle species i and the constant $a$ contains their ground-state spins and mass numbers. In order to make the ratios sufficiently sensitive to the temperature $T$ the double difference of binding energies should be larger than the typical temperature to be measured. For this reason, $^3$He and $^4$He are a useful choice for forming one of the two ratios because the difference in binding energy is 20.6 MeV. It may be combined with, e.g., the lithium yield ratio $^6$Li/$^7$Li or with the hydrogen yield ratios p/d or d/t. Mass spectra obtained for the four isotopes $^3$He, $^4$He, $^6$Li, and$^7$Li from the tracking analysis are shown in Fig. 10. The $^3$He yields reflect the sensitivity of this less strongly bound nuclide to the variation of the temperature with impact parameter.

Solving Eq. (1) with respect to $T$ yields, for the case of He and Li isotopes, the following expression:

$$T_{HeLi,0} = 13.3MeV/\ln(2.2\frac{Y_{^6Li}/Y_{^7Li}}{Y_{^3He}/Y_{^4He}}). \tag{2}$$

The subscript 0 of $T_{HeLi,0}$ refers to the fact that Eq. (1) is strictly valid only for the ground-state population of the considered isotopes at the breakup stage which later may be modified by feeding from the decay of excited states. The temperatures $T_{HeLi,0}$, therefore, will no longer be identical to the breakup temperature. The expected magnitude of this effect was investigated by performing calculations with the quantum statistical model [39]. Results for an assumed density $\rho/\rho_0 = 0.3$ are shown in Fig. 11 ($\rho_0$ denotes the saturation density of nuclei). The relation between $T_{HeLi,0}$ and the input temperature of the model was found to be almost linear which is also the case for, e.g., $T_{Hedt,0}$. Other temperature probes, as illustrated for $T_{Hepd,0}$ in the figure, may be more strongly affected by sequential decays. Variations of the input density within reasonable limits or calculations with other decay models suggested that the accuracy of these estimates may lie within $\pm$ 15% [40].

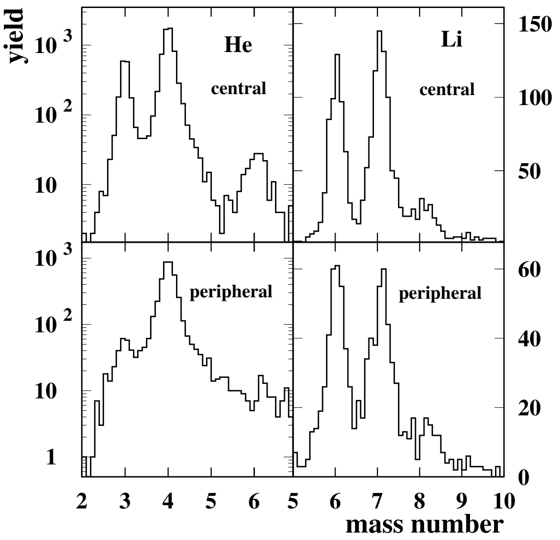


Figure 10: Mass spectra of He fragments (left panel) and Li fragments (right panel) for the reaction $^{197}$Au on $^{197}$Au at $E/A$ = 600 MeV. The upper and lower panels correspond to central and peripheral collisions, respectively (from Ref. [40]).

Based on these findings, the constant correction $T_{HeLi} = 1.2 \cdot T_{HeLi,0}$, corresponding to the dotted line in Fig. 11, was adopted [9].

Temperatures $T_{HeLi}$, as deduced with this method from data measured in three experiments, are shown in Fig. 12 as a function of $Z_{bound}$. Besides the results obtained for the projectile decay in $^{197}$Au on $^{197}$Au collisions at 600 MeV and 1000 MeV per nucleon [9, 40], also temperatures from a more recent study of the target decay in the same reaction at 1000 MeV per nucleon are given [41]. In the latter experiment, $Z_{bound}$ was simultaneously measured for the coincident projectile decay. The temperatures increase slowly with decreasing $Z_{bound}$ in the range $20 \leq Z_{bound} \leq 80$ but then increase more quickly at small $Z_{bound}$ values.

The agreement between the temperatures for the projectile and the target spectators at 1000 MeV per nucleon is expected from the symmetry of the reaction and illustrates the accuracy of the measurements. The invariance with the bombarding energy, here established over the range 600 to 1000 MeV per nucleon, confirms the statistical interpretation of the observed universality of the spectator decay.

The lines shown in Fig. 12 represent results obtained with the statistical multifragmentation model [4]. The excitation energy and mass of the ensemble of excited spectator nuclei, required as input for the calculations, were chosen in such a way that the correlation between the mean multiplicity of intermediate-mass fragments with $Z_{bound}$ (Fig. 5)

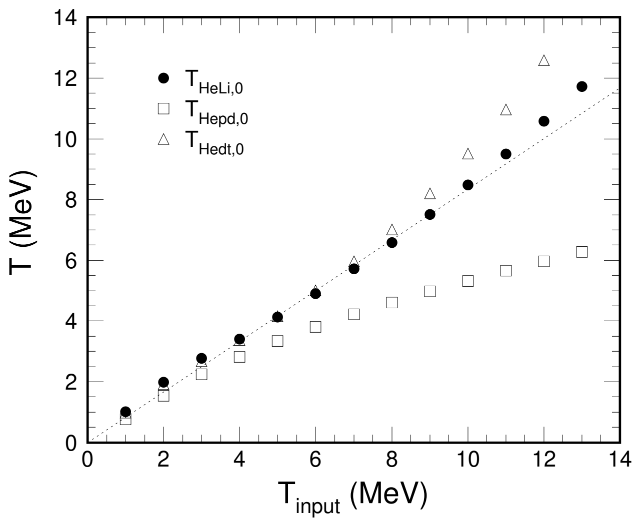


Figure 11: Temperatures $T_{HeLi,0}$, $T_{Hepd,0}$, and $T_{Hedt,0}$, according to the quantum statistical model, as a function of the input temperature $T_{input}$. A breakup density $\rho/\rho_0 = 0.3$ is assumed. The dotted line represents the linear relation $T_{input}/1.2$ (from Ref. [41]).

was well reproduced. Within the given experimental and methodical uncertainties, the resulting mean value of the breakup temperature (full line) is in excellent agreement with the data. This means that the description of the fragmentation as a statistical process is internally consistent in that the temperatures needed to reproduce the observed partition patterns are equal to those measured. The dashed line gives the uncorrected isotopic temperature $T_{HeLi,0}$ deduced from the calculated isotope yields. The difference to the breakup temperature represents the correction for secondary decay according to the statistical multifragmentation model. It is in good qualitative agreement with the adopted correction factor of 1.2.

The consequences of sidefeeding from higher lying states are presently investigated by several groups with different methods [42-47]. The results differ considerably in magnitude as well as in the sign of the required correction and, in some cases, exceed the $\pm 15\%$ margin quoted above. Furthermore, temperatures for central collisions at lower bombarding energies obtained from isotopic yield ratios and from the population of particle-unstable resonances were found to deviate in a systematic fashion from each other [12]. These questions will have to be answered, eventually, in order to maintain a quantitative level in the investigation of thermodynamic properties of excited nuclear systems.

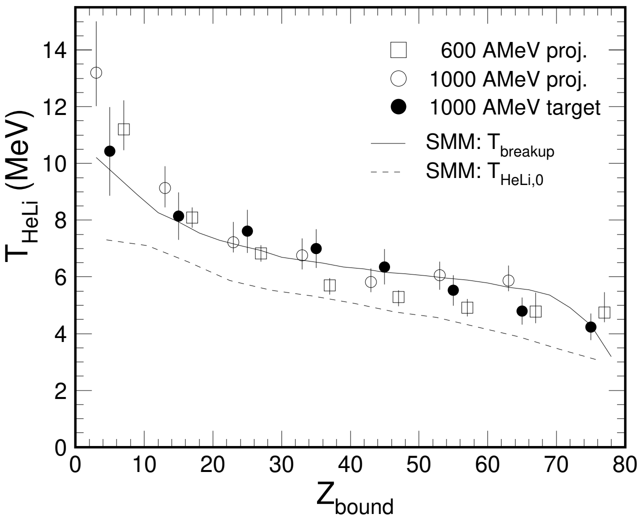


Figure 12: Temperatures $T_{HeLi}$ for target ($E/A$ = 1000 MeV) and projectile spectators ($E/A$ = 600 and 1000 MeV) as a function of $Z_{bound}$. The data symbols represent averages over bins of 10-units width. The full and dashed lines represent the internal temperature $T_{breakup}$ and the uncorrected isotopic temperature $T_{HeLi,0}$ as given by the calculations with the statistical multifragmentation model (from Ref. [41]).

# 6 Energy deposition

Rather small fractions of the initial bombarding energy are imparted to the spectator nuclei in relativistic collisions. The actual amounts of energy deposition can only be reconstructed from the exit-channel configuration which requires a complete knowledge of all decay products, including their atomic numbers, masses, and kinetic energies.

A method to determine the excitation energy from the experimental data along this line was first presented by Campi *et al.* [48] and applied to the earlier $^{197}$Au + Cu data [27]. The yields of hydrogen isotopes were determined by extrapolating to $Z = 1$ from the measured abundances for $Z \geq 2$, and the multiplicities of neutrons were inferred from a mass balance. The obtained asymptotic value of $E_x/A = 23$ MeV at $Z_{bound} = 0$ is the sum of the binding energy of 8 MeV and the kinetic energy of 15 MeV assigned to nucleons.

In the same type of analysis with the more recent data for $^{197}$Au + $^{197}$Au at 600 MeV per nucleon, the data on neutron production measured with LAND were taken into account [9]. Since the hydrogen isotopes were not detected assumptions concerning the overall $N/Z$ ratio of the spectator, the intensity ratio of protons, deuterons, and tritons, and the kinetic energies of hydrogen isotopes had to be made. In addition, the EPAX parameterization [49, 50] was used for deriving masses from the atomic numbers of the detected fragments. The uncertainties resulting from the variation of these quantities within reasonable limits

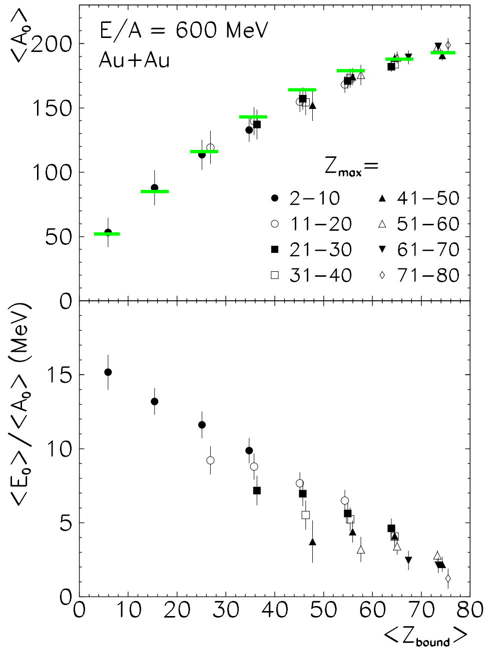


Figure 13: Reconstructed average mass $\langle A_0 \rangle$ (top) and excitation energy $\langle E_0 \rangle / \langle A_0 \rangle$ (bottom) of the decaying spectator system as functions of $Z_{bound}$ (abscissa) and of $Z_{max}$ (different data symbols). The horizontal bars represent the masses according to the participant-spectator model at the empirical impact parameter deduced from $d\sigma/dZ_{bound}$ (from Ref. [9]).

were included in the errors assigned to the results.

It is found that light particles and, in particular, the neutrons contribute considerably to the total spectator energy $E_0$. The balance of binding energies, i.e. the Q value associated with the fragmentation process, amounts to about 40% of it, fairly independent of $Z_{bound}$. The results for the mass $A_0$ and for the specific excitation energy $E_0/A_0$ are given in Fig. 13. The data points represent the results for 10-unit-wide bins in a $Z_{max}$-versus-$Z_{bound}$ representation (cf. Fig. 4). The mean mass $A_0$ decreases with decreasing $Z_{bound}$, seems to be independent of $Z_{max}$, and is in good agreement with the expectations from the geometric participant-spectator model [51]. The smallest mean spectator mass in the bin of $Z_{bound} \leq 10$ is $\langle A_0 \rangle \approx 50$. The excitation energy $E_0$ appears to be a function of both $Z_{bound}$ and $Z_{max}$; the higher values correspond to the smaller $Z_{max}$ values, i.e. to more complete disintegrations of a system of given mass. The maximum number of fragments, observed at $Z_{bound} \approx 40$, is associated with initial excitation energies of $\langle E_0 \rangle / \langle A_0 \rangle \approx 8$ MeV. With decreasing $Z_{bound}$ the deduced excitation energies reach up to $\langle E_0 \rangle / \langle A_0 \rangle \approx 16$ MeV.

The experimentally determined energies fall in between the higher predictions for the deposited energy of the intranuclear cascade model and the much lower values obtained from analyses of the final partitions with the statistical multifragmentation model (Ref. [11] and references therein). A sequence of energies with this ordering is not unreasonable in that the formation of the equilibrated spectator in the initial reaction stages and its evolution towards the final breakup stage may be accompanied by the emission of fast light particles and, therefore, by a loss of excitation energy. On the experimental side, it is presently investigated to what extent the unexpectedly high kinetic energies of protons, preequilibrium emission, and collective phenomena, in particular the bounce-off of the spectator systems, are influencing the deduced energy deposits [30]. The result reported most recently [11] is about 15% higher than that shown in Fig. 13 which entered the caloric curve discussed in the next section.

# 7 The caloric curve

The pairwise correlation of the temperatures and excitation energies, deduced as described in the last two sections, results in the caloric curve shown in Fig. 14. Besides the data from projectile decays following $^{197}$Au + $^{197}$Au collisions at 600 MeV per nucleon, results from earlier experiments with $^{197}$Au targets at intermediate energies 30 to 84 MeV per nucleon and for compound nuclei produced in the $^{22}$Ne + $^{181}$Ta reaction are included [52, 53]. All temperatures were deduced following the same method. For the reactions at intermediate energies, the excitation energy of the target residues was obtained from an energy balance based on moving-source analyses while, in the compound case, it is given by the collision energy.

One may first notice the consistency of the data obtained from different types of reactions, suggesting that the smooth S-shaped curve may represent a more general property of excited nuclei. In fact, at low energies, the deduced temperatures $T_{HeLi}$ follow the low-temperature approximation for a Fermi-liquid, confirmed by several studies in the fusion evaporation regime [54, 55]. The full line depicts this behavior for a level density parameter $a = A/10$ MeV$^{-1}$. At the high excitation energies, the rise of the temperature appears to be linear with the excitation energy, with the slope of 2/3 of a classical gas. In the limit of a free nucleon gas, the offset should be $\approx$ 8 MeV, corresponding to the mean binding energy of nuclei. A smaller offset may be caused by a freeze-out at a finite density and by the finite fraction of bound clusters and fragments of intermediate mass that are present even at these high excitation energies. The offset of 2 MeV is consistent with a breakup density $\rho/\rho_0$ between 0.15 and 0.3 [9]. A final assessment, however, will have to await the completion of the ongoing analysis of the energy deposition.

Within the range of $\langle E_0 \rangle / \langle A_0 \rangle$ from 3 MeV to 10 MeV an almost constant value for $T_{HeLi}$ of about 4.5 to 5 MeV is observed. This plateau may be related to the previous finding

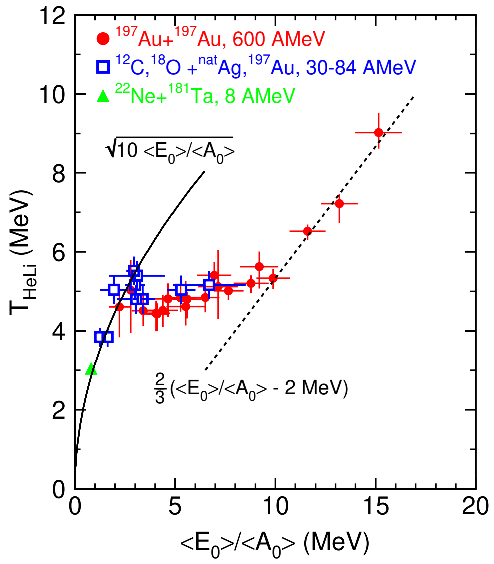


Figure 14: Caloric curve of nuclei as constituted by the temperature $T_{HeLi}$ as a function of the excitation energy per nucleon. The lines are explained in the text (from Ref. [9]).

of almost constant emission temperatures over a broad range of incident energies which were deduced from the population of particle unstable levels in He and Li fragments [32]. The plateau is suggestive of a first-order phase transition with a substantial latent heat (see also [56]). This is supported by the fact that the increase in excitation energy is associated with a disintegration into a larger number of fragments of smaller size as apparent from Fig. 4 ($\langle E_0 \rangle / \langle A_0 \rangle$ has to be translated back into the corresponding $Z_{bound}$ with the help of Fig. 13). The surface energy needed for the formation of smaller constituents limits the rise of the temperature. This interpretation is consistent with the good description of the plateau temperatures by the statistical multifragmentation model which is based on the droplet model of nuclei (Fig. 12).

Alternative interpretations, in particular for the hitherto unobserved temperature rise at the highest energies, have been presented by several groups. The interpretation of Natowitz *et al.* [57] relates the observed variation of the temperature to the variation of the system mass (Fig. 13) and to the mass dependence of the limiting temperatures obtained from theoretical descriptions of excited nuclei at the limit of their stability [58]. In the expansion scenario modeled by Papp and Nörenberg [59], the temperatures in the plateau region are found to be consistent with a spinodal decomposition in the dynamically unstable region of the temperature-versus-density plane. The upbend at high excitation energies, however, indicates a minimum breakup density rather than entry into the vapor phase. The results were found to be sensitive to the equation of state governing the expansion process which presents a further motivation for aiming at a high level of accuracy in these measurements.

# 8 Critical features of multifragmentation

The apparent signatures of a first-order phase transition in nuclei, discussed in the last section, do not rule out the possibility that critical phenomena may be observed. In finite systems, a second-order phase transition is no longer characterized by a singular point, the associated fluctuations are rather spread over a finite interval in temperature [60]. Typical features of a first-order phase transition, like a latent heat, and signals indicating the proximity of the critical point, like diverging moments, are therefore not necessarily inconsistent.

The observation of a power law dependence of the fragment mass yields in reactions of energetic protons with Kr and Xe targets [61, 62], and its association with Fisher's prediction for droplet formation at the critical point [63] has initiated the intensive search for signatures of criticality [2, 16, 64]. The systematic investigations showed that the power law exponent $\tau$ approaches a value of $\approx 2.5$ at high bombarding energies [65]. This is consistent with the limits $2.0 \leq \tau \leq 3.0$ given by the theory of critical phenomena [66]. While the interpretation of inclusive mass spectra was criticized [67], it was shown in exclusive measurements that the mass or charge distributions may approach the pure power law for certain values of the chosen sorting variable, e.g. $Z_{bound}$. In this case, the sorting variable may serve as the parameter controlling the distance to the critical point or critical region. For the fragmentation of $^{197}$Au projectiles at 1 GeV per nucleon, this value is $Z_{bound} \approx 35$ [68] which is close to the maximum fragment production (Fig. 5). Examples of $Z_{bound}$-gated spectra are shown in Ref. [27].

A more recent, equally stimulating, observation was the similarity of the charge fluctuations in fragmentation with those given by three-dimensional percolation on a small lattice [69]. Percolation is a mathematical model exhibiting a second-order phase transition in the limit of infinite lattice size [66]. Campi, therefore, concluded that 'nuclei break up like finite systems that show a clean phase transition in infinite size'. In the meanwhile, it has been demonstrated that nearly perfect descriptions of the partitions observed in multifragmentation reactions may be obtained with the percolation model [27].

The capability of percolation to describe the partition space is not trivial but it is also not unique to percolation. The fragment-charge correlations from the first experiments have been reproduced to high accuracy with the statistical multifragmentation model, but also with a variety of other models, such as classical-cluster formation [70], fragmentation-inactivation binary [71], and restructured-aggregation models [72]. Some of these models exhibit critical behavior in the limit of an infinite number of constituents. The apparent universality, inherent to disordered systems of interacting nucleons and to the models describing their fragmenting so well, remains to be understood [73].

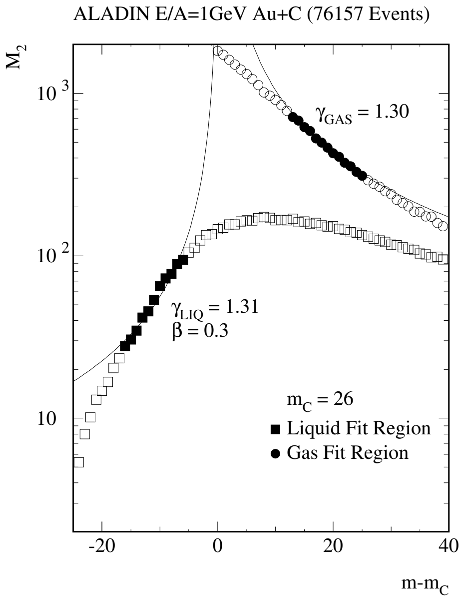


Figure 15: Second moment $M_2$ of the fragment-charge distribution, with (circles) and without (squares) including the largest fragment, as a function of the charged particle multiplicity $m$ for $^{197}$Au + C at $E/A$ = 1 GeV. The assumed critical multiplicity is $m_c$ = 26, the full symbols indicate the selected fit regions (from Ref. [68]).

A further step was taken by the EOS collaboration who have reported values for critical-point exponents from the charge correlations measured for the $^{197}$Au on C reaction at 1 GeV per nucleon [10, 74, 75]. The analysis takes extensive recourse to results obtained for percolation. Below the critical point, the largest cluster of the partition is associated with the percolating cluster which corresponds to the liquid phase in a liquid-gas transition. It grows in proportion to $t^\beta$ with the relative distance $t$ from the critical point. The role of the susceptibility in magnetic systems or the isothermal compressibility in a liquid, i.e. the response to the external field, is assumed by the second moment $M_2$ of the fragment size distributions. It diverges with the power of -$\gamma$ as the critical point is approached (both $\beta$ and $\gamma$ are positive numbers).

With the guidance provided by percolation studies on small lattices, recipes were developed on how to extract critical exponents from the data [76]. The reported results $\beta = 0.29 \pm 0.02$ and $\gamma = 1.4 \pm 0.1$ are close to those of a liquid-gas system and significantly different from those of percolation or mean-field theory [10]. This conclusion relies on the correct assessment of the systematic errors inherent to the procedure which, however, has been questioned by other authors [77, 78]. A critical discussion may also be found in the contributions to Refs. [14, 16] by Müller *et al.* who, besides percolation, have studied Ising models on small lattices.

A critical-exponent analysis has been carried out with the ALADIN data for $^{197}$Au and $^{238}$U fragmentations [68]. The same numerical results were obtained if the procedure of Ref. [10] was followed in detail. However, also the same difficulties arising from the finite system size were encountered. As an example, the fits used to extract the exponent $\gamma$ are shown in Fig. 15. The figure is virtually identical to the corresponding figure constructed from the EOS data [79]. Potential divergences at the critical point that will appear in the infinite system are smoothed over finite regions of the chosen control parameter, the charged particle multiplicity $m$. The choice of the fit regions where the data are assumed to reflect the critical behavior is crucial. It has to rely on methods obtained from the study of other systems which, at this time, are not yet proven unambiguous. A consistent method was found for determining the exponent $\tau$ of the power law obeyed by the element distribution [68]. This may be related to the fact that $\tau$ describes a behavior *at* the critical point, and not the behavior how the critical point is approached. The finite size of the system may be less crucial in this case.

# 9 Conclusions and perspectives

The systematic set of data now available reveals the universal nature of multi-fragment decays of excited spectator nuclei at relativistic energies. It suggests that the correlation of excitation energy and mass of the produced spectator systems and the statistical nature of their decay are independent of the specific entrance channel. The emulsion data as well as the insight provided by calculations indicate that it should prevail up to very high bombarding energies with virtually unchanged features. There are lower limits of the bombarding energy below which the spectator excitation does not suffice to induce a complete disassembly with maximum fragment production. These threshold energies depend on the collision partner, as shown for the case of gold nuclei in Fig. 16. Besides data measured with the ALADIN spectrometer in inverse kinematics, also data for $^{197}$Au on $^{197}$Au at lower energies [80], for $^{84}$Kr on $^{197}$Au [81], and for $^{4}$He on $^{197}$Au [82] are included. The hatched line indicates these threshold energies as a function of the target mass. If the bombarding energy is raised above the threshold, the maximum fragment production will shift to more peripheral collisions. Below the threshold, the production of heavy residues will be the dominating process.

As one moves along the hatched line towards the central collisions of heavy systems,

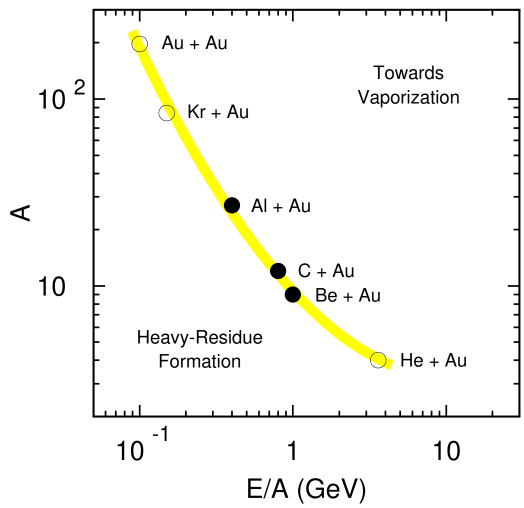


Figure 16: Mass number $A$ of the collision partner versus bombarding energy for reactions of $^{197}$Au nuclei for which maximum fragment production has been observed in central collisions (from Ref. [11]).

dynamical phenomena become important. The largest fragment multiplicities measured so far were observed in central $^{197}$Au on $^{197}$Au collisions at a bombarding energy of 100 MeV per nucleon [80]. The analysis of the kinetic energy spectra in these reactions has revealed a considerable collective outward motion (radial flow), superimposed on the random motion of the constituents at the breakup stage [83]. The associated collective energy constitutes up to one-half of the incident kinetic energy in the center-of-mass frame and increases approximately linearly over the range of bombarding energies up to 1000 MeV per nucleon [84]. Furthermore, the fragment formation was found to be sensitive to the flow dynamics. The measured element yields are systematically correlated with the magnitude of the observed radial flow [84, 85].

This excursion to central collisions, not covered in the main part of these notes, is meant to demonstrate that heavy ion reactions at relativistic energies offer wide possibilities to study the response of excited nuclear matter under different conditions. The interplay of dynamical and statistical effects in these violent central collisions is of high current interest [86]. The measurement of breakup temperatures for these reactions, where equilibrium may be established only locally, has already been started and promises to produce stimulating new results [12].

Large dynamical effects are not expected in light-particle induced reactions with heavy targets, i.e. at the lower end of the hatched line in Fig. 16. Here the main problem arises from the fact that the cross sections for large energy transfers to the target with maximum fragment production are comparatively small [82, 87, 88]. New experimental results including exclusive measurements with beams of antiprotons [89] and of protons with energies up to 14 GeV [90] have been obtained very recently, and a comprehensive picture of the light-ion reactions should emerge rather soon.

The phenomenology of multifragment-decays, in particular the partitioning of the decaying systems, has been established with high accuracy, as shown in the first part of these notes. The critical discussion of the new methods for measuring thermodynamic properties of excited nuclear systems is important. Here the systematic errors will have to be further reduced, which seems feasible with improved experiments and model calculations. The search for critical phenomena has to take the small number of constituents into account, and concepts developed for macroscopic systems have to be applied with caution. The finite system size, on the other hand, offers wide possibilities for model studies based on different approaches, aiming at an understanding of the universal properties of nuclear fragmentation and of fragmentation and clustering phenomena in other fields.

*I am highly indebted to my colleagues of the ALADIN collaboration for valuable discussions and support during the preparation of this manuscript.*

# References

[1] P.J. Siemens, *Nature (London)* 305: 410 (1983).

[2] J. Hüfner, *Phys. Rep.* 125: 129 (1985).

[3] D.H.E. Gross, *Rep. Prog. Phys.* 53: 605 (1990).

[4] J.P. Bondorf *et al.*, *Phys Rep.* 257: 133 (1995).

[5] H. Jaqaman *et al.*, *Phys. Rev.* C 27: 2782 (1983) .

[6] M. Brack *et al.*, *Phys. Rep.* 123: 275 (1985).

[7] G. Bertsch and P.J. Siemens, *Phys. Lett.* 126 B: 9 (1983) .

[8] W. Stocker, *Phys. Lett.* 142 B: 319 (1984) .

[9] J. Pochodzalla *et al.*, *Phys. Rev. Lett.* 75: 1040 (1995) .

[10] M.L. Gilkes *et al.*, *Phys. Rev. Lett.* 73: 1590 (1994) .

[11] A. Schüttauf *et al.*, *Nucl. Phys.* A 607: 457 (1996) .

[12] for the most recent reports of the collaboration see, e.g.,
G. Immé *et al.*, to appear in *Proceedings of the 1st Catania Relativistic Ion Studies: Critical Phenomena and Collective Observables*, Acicastello, Italy, 1996;
W.F.J. Müller *et al.*, ibid.;
J. Pochodzalla *et al.*, ibid.

[13] *Proceedings of the International Workshop XXII*, Hirschegg, 1994, edited by H. Feldmeier and W. Nörenberg (GSI, Darmstadt, 1994).

[14] *Proceedings of the XXXIII International Winter Meeting on Nuclear Physics*, Bormio, 1995, edited by I. Iori (Ricerca Scientifica ed Educazione Permanente, Milano, 1995).

[15] *Proceedings of the 12th Winter Workshop on Nuclear Dynamics*, Snowbird, Utah, USA, 1996.

[16] *Proceedings of the 1st Catania Relativistic Ion Studies: Critical Phenomena and Collective Observables*, Acicastello, Italy, 1996.

[17] For a recent review see L.G. Moretto and G.J. Wozniak, *Ann. Rev. Nucl. Part. Science* 43: 379 (1993).

[18] B. Jakobsson *et al.*, *Z. Phys.* A 307: 293 (1982) .

[19] E.M. Friedlander *et al.*, *Phys. Rev.* C 27: 2436 (1983) .

[20] P.L. Jain *et al.*, *Phys. Rev.* C 50: 1085 (1994) .

[21] M.L. Cherry *et al.*, *Phys. Rev.* C 52: 2652 (1995) .

[22] G. Rusch *et al.*, *Phys. Rev.* C 49: 901 (1994) .

[23] J. Hubele *et al.*, *Z. Phys.* A 340: 263 (1991) .

[24] W.D. Kunze, PhD thesis, Universität Frankfurt, 1996, unpublished.

[25] C.A. Ogilvie *et al.*, *Phys. Rev. Lett.* 67: 1214 (1991) .

[26] J. Hubele *et al.*, *Phys. Rev.* C 46: R1577 (1992) .

[27] P. Kreutz *et al.*, *Nucl. Phys.* A 556: 672 (1993) .

[28] Y. Yariv and Z. Fraenkel, *Phys. Rev.* C 20: 2227 (1979) ; *Phys. Rev.* C 24: 488 (1981) .

[29] V.S. Barashenkov and V.D. Toneev, Interactions of high-energy particles and atomic nuclei with nuclei, Moscow, Atomizdat, 1972 (in Russian);
V.D. Toneev, private communication (1994).

[30] A. Schüttauf, PhD thesis, Universität Frankfurt, 1996, unpublished.

[31] V. Lindenstruth, PhD thesis, Universität Frankfurt, 1993, report GSI-93-18.

[32] G.J. Kunde *et al.*, *Phys. Lett.* B 272: 202 (1991) .

[33] H.W. Barz *et al.*, *Phys. Lett.* B 217: 397 (1989) .

[34] D.H. Boal *et al.*, *Phys. Rev. Lett.* 62: 737 (1989) .

[35] H.W. Barz *et al.*, *Phys. Lett.* B 228: 453 (1989) .

[36] W. Bauer, *Phys. Rev.* C 51: 803 (1995) .

[37] D. Morrissey *et al.*, *Ann. Rev. Nucl. Part. Science* 44: 27 (1994).

[38] S. Albergo *et al.*, *Il Nuovo Cimento* 89 A: 1 (1985).

[39] J. Konopka *et al.*, *Phys. Rev.* C 50: 2085 (1994) .

[40] T. Möhlenkamp, PhD thesis, Universität Dresden, 1996, unpublished.

[41] Hongfei Xi *et al.*, to be published.

[42] M.B. Tsang *et al.*, *Phys. Rev.* C 53: R1057 (1996) .

[43] A. Kolomiets *et al.*, *Phys. Rev.* C 54: R472 (1996) .

[44] X. Campi *et al.*, *Phys. Lett.* B, in print.

[45] M.B. Tsang *et al.*, preprint MSUCL-1035 (1996).

[46] Hongfei Xi *et al.*, preprint MSUCL-1040 (1996).

[47] Z. Majka *et al.*, preprint 96-03, Texas A&M University (1996).

[48] X. Campi *et al.*, *Phys. Rev.* C 50: R2680 (1994) .

[49] K. Sümmerer *et al.*, *Phys. Rev.* C 42: 2546 (1990) .

[50] A.S. Botvina *et al.*, *Nucl. Phys.* A 584: 737 (1995) .

[51] J. Gosset *et al.*, *Phys. Rev.* C 16: 629 (1977) .

[52] R. Trockel *et al.*, *Phys. Rev.* C 39: 729 (1989) ; R. Trockel, PhD thesis, Universität Heidelberg, 1988, unpublished.

[53] C. Borcea *et al.*, *Nucl. Phys.* A 415: 169 (1984) .

[54] G. Nebbia *et al.*, *Phys. Lett.* B 176: 20 (1986) .

[55] D. Fabris *et al.*, *Phys. Lett.* B 196: 429 (1987) .

[56] L.G. Moretto *et al.*, *Phys. Rev. Lett.* 76: 2822 (1996) .

[57] J.B. Natowitz *et al.*, *Phys. Rev.* C 52: R2322 (1995) .

[58] P. Bonche *et al.*, *Nucl. Phys.* A 436: 265 (1986) .

[59] G. Papp and W. Nörenberg, preprint GSI-95-30 (1995).

[60] A.L. Goodman *et al.*, *Phys. Rev.* C 30: 851 (1984) .

[61] J.E. Finn *et al.*, *Phys. Rev. Lett.* 49: 1321 (1982) .

[62] A.S. Hirsch *et al.*, *Phys. Rev.* C 29: 508 (1984) .

[63] M.E. Fisher, *Physics (N.Y.)* 3: 255 (1967).

[64] J. Richert, *Int. J. Mod. Phys.* E2: 679 (1993).

[65] W. Trautmann *et al.*, *Z. Phys.* A 344: 447 (1993) .

[66] D. Stauffer and A. Aharony, *Introduction to Percolation Theory*, Taylor & Francis, London (1992).

[67] J. Aichelin *et al.*, *Phys. Rev.* C 37: 2451 (1988) .

[68] A. Wörner, PhD thesis, Universität Frankfurt, 1995, unpublished.

[69] X. Campi, *Phys. Lett.* B 208: 351 (1988) .

[70] J.B. Garcia and C. Cerruti, *Nucl. Phys.* A 578: 597 (1994) .

[71] R. Botet and M. Ploszajczak, *Phys. Lett.* B 312: 30 (1993) ; *Acta Physica Polonica* B25: 353 (1994).

[72] S. Leray and S. Souza, *Proceedings of Second European Biennial Conference on Nuclear Physics*, Megève 1993, edited by D. Guinet (World Scientific, Singapore, 1995) p. 81.

[73] B. Elattari *et al.*, *Phys. Lett.* B 356: 181 (1995) ; *Nucl. Phys.* A 592: 385 (1995) .

[74] J.A. Hauger *et al.*, *Phys. Rev. Lett.* 77: 235 (1996) .

[75] J.B. Elliott *et al.*, *Phys. Lett.* B 381: 35 (1996) .

[76] J.B. Elliott *et al.*, *Phys. Rev.* C 49: 3185 (1994) .

[77] W. Bauer and W.A. Friedman, *Phys. Rev. Lett.* 75: 767 (1995) .

[78] W. Bauer and A.S. Botvina, *Phys. Rev.* C 52: R1760 (1995) .

[79] H.G. Ritter *et al.*, *Nucl. Phys.* A 583: 491c (1995) .

[80] M.B. Tsang *et al.*, *Phys. Rev. Lett.* 71: 1502 (1993) .

[81] G.F. Peaslee *et al.*, *Phys. Rev.* C 49: R2271 (1994) .

[82] V. Lips *et al.*, *Phys. Rev. Lett.* 72: 1604 (1994) .

[83] W.C. Hsi *et al.*, *Phys. Rev. Lett.* 73: 3367 (1994) .

[84] W. Reisdorf *et al.*, in Ref. [13], p.93.

[85] G.J. Kunde *et al.*, *Phys. Rev. Lett.* 74: 38 (1995) .

[86] J. Bondorf *et al.*, *Phys. Rev. Lett.* 73: 628 (1994) .

[87] K. Kwiatkowski *et al.*, *Phys. Rev. Lett.* 74: 3756 (1995) .

[88] L. Pienkowski *et al.*, *Phys. Lett.* B 336: 147 (1994) .

[89] F. Goldenbaum *et al.*, *Phys. Rev. Lett.* 77: 1230 (1996) .

[90] V.E. Viola *et al.*, *Proceedings of Third International Conference on Nuclear Physics at Storage Rings*, Bernkastel-Kues, Germany, 1996.